High frequency edge coherent modes studied with the ultra-fast swept reflectometer on ASDEX Upgrade

A. Medvedeva[1,2], C. Bottereau[1], F. Clairet[1], G. D. Conway[2], P. Manz[2] , F. Mink[2] , V. Nikolaeva[5], D. Prisiazhniuk[2], U. Stroth[2,4], E. Wolfrum[2], A. Biancalani[2], S. Heuraux[3], D. Molina[1], A. Silva[5], ASDEX Upgrade Team[2] and EUROfusion MST1 team[a]

[1] CEA, IRFM, 13108 St-Paul-Lez-Durance, France
[2] Max-Planck-Institut für Plasmaphysik, 85748 Garching, Germany
[3] Institut Jean Lamour UMR 7198 CNRS, Université de Lorraine, BP 50840, 54011, France
[4] Physik-Department E28, Technische Universität München, 85747 Garching, Germany
[5] Instituto de Plasmas e Fusão Nuclear, IST, Universidade Lisboa, Lisbon, Portugal
[a] For a list of members, see H.Meyer et al, Nucl. Fusion 57 102014 (2017)

Abstract. The results on high frequency coherent modes developing at the plasma edge after L-H transitions are presented. These edge coherent modes (ECMs) observed in the I-phase, during ELM-free and ELMy H-mode phases have common characteristics, such as their frequency of 50–200 kHz, radial position and scaling of the frequency with the pressure gradient. The ultra-fast swept reflectometer with the sweep time of 1 μs has provided measurements of the mode dynamics and localisation. The ECMs propagate in the electron diamagnetic direction in the laboratory frame and are localized in the region between the pedestal top and the steepest pressure gradient.

Keywords: magnetic confinement, plasma physics, fusion, turbulence, L-H transition, coherent modes

1. Introduction

The modes which can be observed in a confined magnetized plasma are related to instabilities caused by different drives, like pressure gradient or fast particles. During the transition from L- to H-mode the strong pressure gradient establishing in the edge triggers various instabilities which may play a role in the building of the pedestal. In order to identify such instabilities it is important to characterise their basic properties, which can be measured in the experiment: the growth rate, the poloidal and toroidal mode numbers m, n, the mode frequency ω and the modes' radial structure.

Previous experiments on different devices reported the onset of high frequency coherent modes with $f > 40$ kHz in the plasma edge region in high confinement regimes [1, 2, 3, 4, 5, 6]. The underlying instabilities need to be investigated as they could be the reason for the limitation of the pedestal gradients after the transition to the improved confinement. The list of possible candidates includes kinetic ballooning modes [4] (KBM), resistive ballooning modes [1, 7] (RBM) or microtearing modes [8] (MTM). In EAST the edge coherent modes were identified as trapped electron modes (TEM) [9]. In the H-mode, quasi-coherent modes with typical frequencies of about 100 kHz are thought to play a role in the inter-ELM dynamics by clamping the pressure gradient. These modes are considered to have a KBM nature [10, 11]. Quasi-coherent modes observed in Alcator C-Mod matched the resistive ballooning coherent modes simulated in three dimensional electromagnetic fluid codes[12]. The modes with multiple branches in the range around 100 kHz can also be Alfvén frequency modes, as seen in neutral beam heated and in Ohmic plasmas in TFTR tokamak [13] for instance. Thus several types of oscillations with similar properties can manifest during and after the transition to the H-mode and the experimental evidence may help to distinguish between various interpretations.

This contribution summarises the results obtained in a study of coherent modes in AUG which have common characteristics, such as their frequency range of 50–200 kHz and their edge radial position, and thus will be grouped under the name of edge coherent modes (ECM). They appear in different plasma confinement regimes, such as the I-phase [14, 15] or ELM-free and ELMy H-modes. Section 3.1 describes the general observations, section 3.2 present the analysis of the modes' behaviour during the ELM-free phase of the H-mode and the ELMs. In section 3.3 modes' nature is discussed.

2. Methods

The mode numbers and frequency can be calculated from the analysis of magnetic pick-up coil signals giving the temporal derivative of the magnetic field components B_r or B_θ. The main disadvantage of the pick-up coils is their non-local measurement

outside the plasma, related to their position. Therefore only modes with high amplitude can be detected and they need an electromagnetic component to be detectible outside the plasma. In addition the magnetic component can be screened by the plasma. However, this diagnostic has several advantages: simple calibration, high sensitivity ($10^{-4} - 10^{-5}$ T) and a high number of coils available at different poloidal and toroidal locations [16]. The system of pick-up coils in AUG includes two poloidal sets of 32 Mirnov's coils and additionally 5 coils mounted at different toroidal positions close to the mid plane measuring $\dot{B}_\theta$, one toroidal set of 8 coils measuring $\dot{B}_r$.

Modes can be detected by reflectometry diagnostics in the frequency spectrum of the reflected signal. In contrast to the Mirnov coils this measurement has a local character. Using several probing wave frequencies, the mode can be localised radially. In AUG two systems of profile reflectometry and a poloidal correlation reflectometer are installed, which will be introduced in the following.

The FM-CW reflectometer in O-mode in the sector 6 provides electron density profiles by sweeping the probing frequency in 20 μs. It has antennas installed both on the low magnetic field side (LFS) and the high field side (HFS). The same system can be programmed for a fixed probing wave frequency and therefore it can produce density fluctuation frequency spectra [17]. The main characteristic of density measurements by reflectometry is the high sub-centimetre precision of the profile allowing a precise calculation of the local gradients.

The ultra-fast swept reflectometer (UFSR) recently transfered from Tore Supra to AUG has provided electron density profile measurements with a time resolution of 1 μs. The system consists of V and W band (50–105 GHz) frequency sweeping reflectometers [18]. The emitting and receiving bistatic antennas are installed on the mid plane of AUG at the low-field side with a line of sight in radial direction towards the centre of the plasma. The frequency bands of the probing waves are chosen such that the signal propagates from the low-field side into the plasma until it is reflected at the cut-off layer with the X-mode upper cut-off frequency

$$\omega_+ = \frac{\Omega_{ce}}{2}\left(1 + \sqrt{1 + \frac{4\omega_p^2(n_e)}{\Omega_{ce}^2}}\right), \tag{1}$$

where $\omega_p^2 = n_e e^2/\epsilon_0 m_e$ and $\Omega_{ce} = eB/m_e$, with the electron density n_e, electron mass m_e and magnetic field strength B. The X-mode polarisation provides a large radial access from the very edge to the centre of the plasma for densities up to $5 \cdot 10^{19}$ m^{-3}. Using a linear frequency sweep and an iterative Bottollier-Curtet procedure [19] a density profile can be obtained. The turbulent plasma density fluctuations can be extracted from the fluctuations of the reflected signal [20]. The heterodyne receiver and IQ detection assure a separation of phase and amplitude of the reflected signal with a signal to noise ratio of about 40 dB, sufficient for fluctuation measurements. Fast and repetitive sweeps of 1 μs with 0.25 μs dead time between sweeps provide an equivalent sampling rate of 800 kHz at a given probing frequency. The frequency spectra are obtained by taking the FFT of the complex signal $S = A(t)e^{i\Phi(t)}$ for each probing frequency. For a fixed radial

position, this permits frequency spectra reconstruction up to a half of the sampling frequency $\frac{1}{2}f_s = \frac{1}{2}(t_{sweep} + t_{dead})^{-1}$ equal to 166 kHz for the 2014-2015 campaign and 400 kHz since 2016. The time window length for the spectrum reconstruction has to be adjusted according to the phenomena time scale. There is always a competition between the time resolution and the reduction of noise in the spectra which can be reduced by ensemble averaging of several spectra. Applying a fast Fourier transform (FFT) to successive time windows, the temporal development of the power spectrum can be obtained and represented as a spectrogram which provides a good overview of the modes dynamics in frequency and amplitude. Thanks to the reconstruction of density profiles, the probing frequency can be expressed as a monotonic function of the radial position $F(R)$. Hence the complex signal can be interpolated to the radial points of the averaged density profile.

Poloidal correlation reflectometry (PCR) provides measurements of the mode's velocity and poloidal size, which allows the identification of the mode number. In addition the temporal dynamics can be studied on a time scale of the window used in the FFT. The PCR system on AUG [21] consists of one emitting and 4 receiving antennas separated poloidally and toroidally. The mode perpendicular wavenumber $k_\perp$ is found from the ratio of phase difference between the oscillation's maxima for a pair of antennas to the poloidal separation between these antennas. The poloidal velocity in the laboratory frame for a mode with frequency f is estimated as $v_\perp = 2\pi f/k_\perp$ and the toroidal mode number can be determined as $n = R_0 k_\perp \sin(\alpha)$, where α is a pitch angle and R_0 the radial position of the mode.

3. Experimental results

3.1. Observation of modes with the UFSR

Different edge coherent modes (ECMs) have been detected in the reflectometer signals during the experiments dedicated to L-H transition studies on AUG [22]. First appearing as sequences of pulsations in the raw reflectometer phase signal the modes could later be visible in the frequency spectra. Almost in all cases the modes start to be visible in the pick-up coil signals a few milliseconds later and therefore have an electromagnetic nature. The modes have been observed in the UFSR signal continuously during the I-phase, after the transition to the ELM-free phase of the H-mode and in between ELMs. The mode frequency is in the range of 40–200 kHz and often several branches are observed simultaneously. This observation is similar to Alfvén eigenmodes [23, 24]. However, the latter are usually observed when NBI creates a population of fast particles, while the modes studied here were also found in discharges without NBI. This feature necessitates to question more accurately their nature. ECMs were previously investigated in AUG in between ELMs, although they were not yet decisively identified [6, 5].

Figure 1 illustrates the development of ECMs after the L-mode (a) during the I-phase (b) and in H-mode (c) in a low density discharge #31287 with 1.6 MW of ECRH.

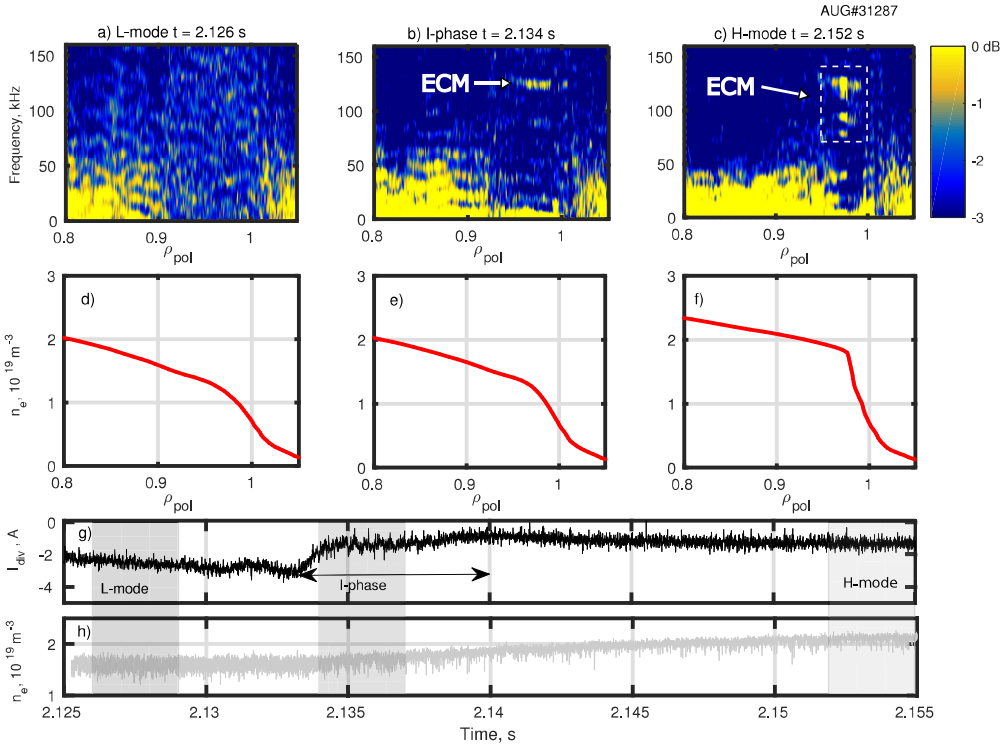

Figure 1. Density fluctuation frequency power spectra in (a) L-mode, (c) H-mode and (b) during I-phase, corresponding electron density profiles (d-f), divertor current indicating the confinement transition (g) and pedestal top density (h), shaded area correspond to the time windows used for the calculation of the spectra

In the pedestal region during the I-phase the density fluctuation amplitude decreases and the spectra become narrower compared to typical L-mode spectra (Fig. 1a) which are more broadband. Modes at about 120 kHz start to grow directly at the transition from the L-mode to the I-phase in the edge region $0.95 < \rho_{pol} < 0.99$ (Fig. 1b,e) and their amplitude saturates during the ELM-free phase of the H-mode (Fig. 1c). The oscillations occur within the range of 60–80 GHz of UFSR probing frequencies, corresponding to the edge region inside the separatrix. In between ELMs the modes become saturated again and disappear during ELM crashes. An important feature of these modes is their coherency, meaning that in the frequency spectrum they have a distinctive narrow peak above the noise level with a width $\Delta f \ll f$. At the same time, the rest of the usual broad L-mode spectrum is suppressed when the modes increase in amplitude. Summarising the aforementioned characteristics, the modes were named edge coherent modes [25].

Note that the radial position for each spectrum is defined from a bijective relation $\langle F_{prob,i}(t) \rangle \leftrightarrow \langle R_i(t) \rangle$ where the probing frequency F_{prob} and corresponding radial positions R_i are averaged over the FFT time window of typically a few milliseconds. In the example of Fig. 1 this window was 3 ms and included 1000 consecutive frequency sweeps. Figure 2a shows an example of the frequency spectra for all probing frequencies. The ECMs are visible between 70 and 125 kHz for the probing frequencies of 67–75 GHz.

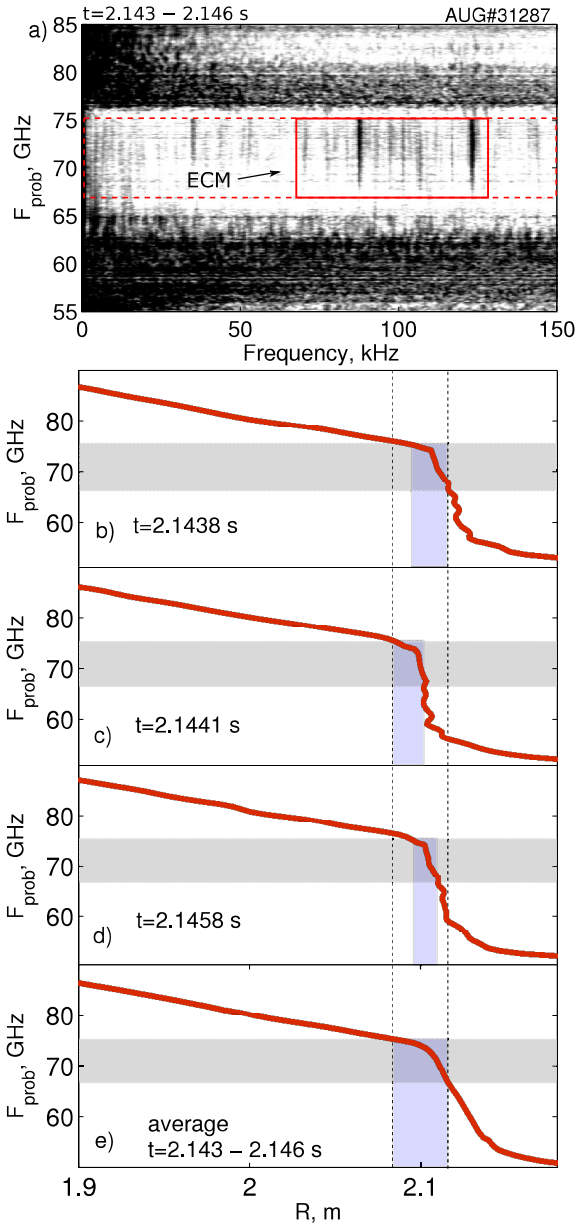

Figure 2. (a) Frequency spectra for all probing frequencies during the I-phase AUG#31287. The ECMs are measured with probing frequencies of 67–75 GHz within the time window t =2.143–2.146 s of typical FFT, corresponding to the region from the strong gradient localisation to the top of the pedestal. Absolute position of UFSR measurement for different probing frequencies is shown in (b-e), as individual profiles (b-d) and in average over 3 ms(e). Blue rectangles demonstrate how the probing frequency range can be interpreted in terms of radial position (b-d) and create an additional broadening of the mode localisation (e)

Figure 2b-d depicts the dependence of the absolute radial position from the probing frequency for 3 different sweeps. The probing frequencies of 67–75 GHz (shaded area) clearly correspond to the top of the pedestal and the upper part of the gradient region

as it is shown in Figs. 2b-d with the blue rectangles, the absolute position is around 2.10 m, while the magnetic axis of the plasma is at 1.675 m and the separatrix position is at 2.14 m at the mid plane. Due to the density profile dynamics during 3 ms each reflectometer frequency $F_{prob,i}$ probes a different radial position from one sweep to the next around an average position $\langle R_i \rangle$, hence the actual shift of the profile can introduce an additional extension of the estimated mode position when the interpolation is made for the average profile $F(R)$ (Fig. 2e). The radial extension over which the mode affects the reflectometer signal is within 1.5 cm in the edge for each individual profile (Fig. 2b-d), which is about 0.03 in terms of normalised radius ρ_{pol}. However, when the average profile is plotted, the modes seem to be located in a region of 2.5 cm with significantly broader contribution of the pedestal top, which is misleading.

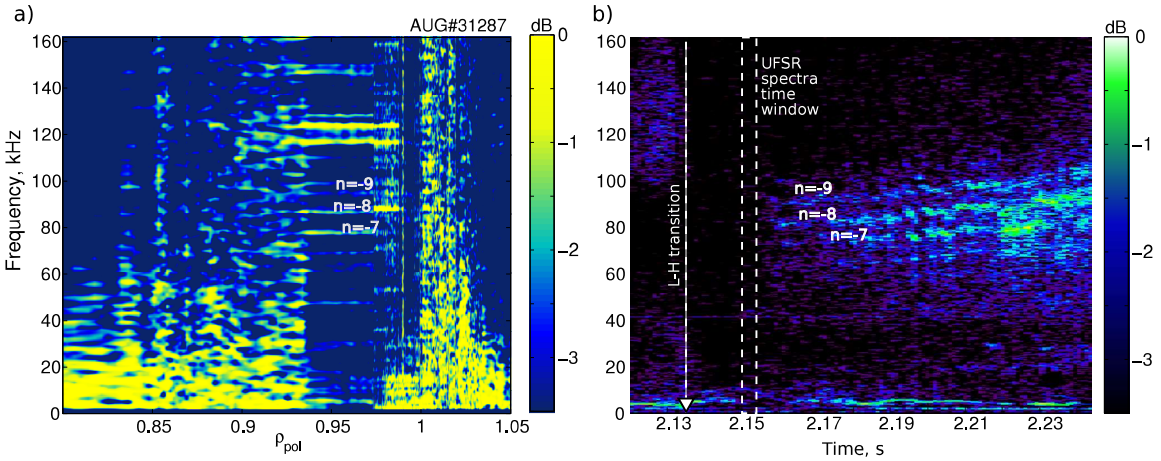

Figure 3. Frequency spectra of the discharge #31287 from UFSR at 2.150–2.153 s (a) and a spectrogram from the pick-up coil, the start of the L-H transition is indicated with the white arrow (b)

The magnetic pick-up coils were used to deduce the toroidal mode numbers as described in [26]. When examining the pick-up coil spectrogram, the modes are not yet visible during the first 18 ms after the L-I-phase transition (Fig. 3b). They appear in the spectrogram only after $t = 2.15$ s with branches around 65–105 kHz. The mode at 125 kHz is not visible in the magnetic pick-up coils while being clearly observed with the UFSR. The toroidal mode numbers vary between $n = -5$ and -10 (Fig. 3a) for the lowest to the uppermost branch (the negative sign corresponds to the electron diamagnetic direction in the laboratory frame). Usually the distance between the coils does not allow to detect mode numbers higher than 25 [6]. The most pronounced branches in the magnetic pick-up coil spectrum correspond to $n = -6$ and -7 at frequencies of 65–80 kHz, while in the UFSR signal the modes with frequencies of 115–125 kHz have the strongest amplitude. The UFSR frequency spectra (Fig. 3a) are constructed for the window 2.150–2.153 s. The modes' locations slightly vary with mode number: $n = -7$ is more visible at the top of the pedestal $0.93 < \rho_{pol} < 0.96$ while $n = -9$ is shifted to the gradient region $0.97 < \rho_{pol} < 0.99$. Assuming the same propagation velocity for the mode visible in the spectra with a frequency around 125 kHz and the modes with $n = -7$ to -9, the corresponding mode number would

be $n = -12$, not detected in the pick-up coil analysis. Similar modes with toroidal mode numbers from $n = -3$ to -12 and poloidal mode numbers around $m = 30$ for the lower n numbers were described in [26] as MHD activity between ELM bursts in AUG. Their position was estimated by matching their frequency and mode number to the q-profile and the background $\mathbf{E} \times \mathbf{B}$ velocity and was found to be between the E_r minimum and the separatrix. The UFSR system identifies these modes in the narrow region of pedestal top and in the gradient region.

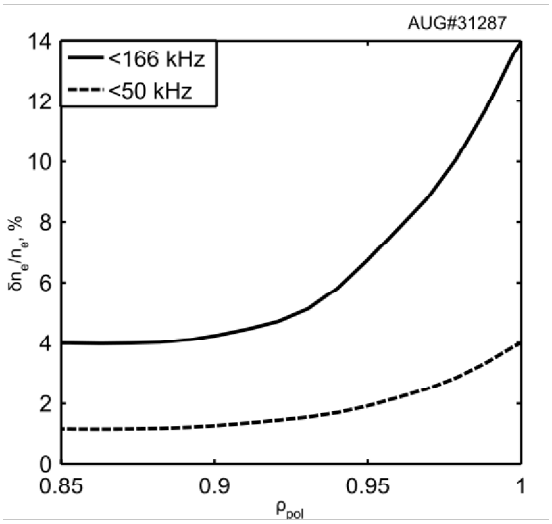

Figure 4. Density fluctuation level for frequencies $f < 166$ kHz (solid) and $f < 50$ kHz (dashed) in the ELM-free phase of the H-mode with ECMs, $t = 2.141$ s

The analysis of the density fluctuations becomes complicated as the coherent modes dominate the turbulent spectrum. In order to distinguish density fluctuations due to these modes and broadband turbulence, a low-pass filter $f < 50$ kHz, filtering out the ECM, has been applied to the UFSR signal phase. The density fluctuation profile shape is unchanged after filtering (Fig. 4), the absolute level of density fluctuations decreases proportionally to the filter width, hence the ECMs do not contribute to the selected k_r range from 2 to 20 cm^{-1}. The calculation of the density fluctuation level here uses the closed-loop method where the wavenumber spectra are reconstructed and then integrated over a selected range of k_r. That indicates that the edge coherent modes have a small radial wavenumber $k_r < 2$ cm^{-1}, corresponding to a size of about 1.5 cm which is consistent with the mode's width in Fig.1.

Summarising the observations, ECMs are localised in the edge region $0.92 < \rho_{pol} < 0.99$, with indications from the UFSR that they are mostly located in the gradient region. The toroidal mode numbers change from -5 to -12 and the modes propagate in the electron diamagnetic direction in the laboratory frame. The ECMs have a small radial wavenumber $k_r < 2$ cm^{-1}. They saturate after the transition to the I-phase or the H-mode and disappear only during and shortly after ELM crashes.

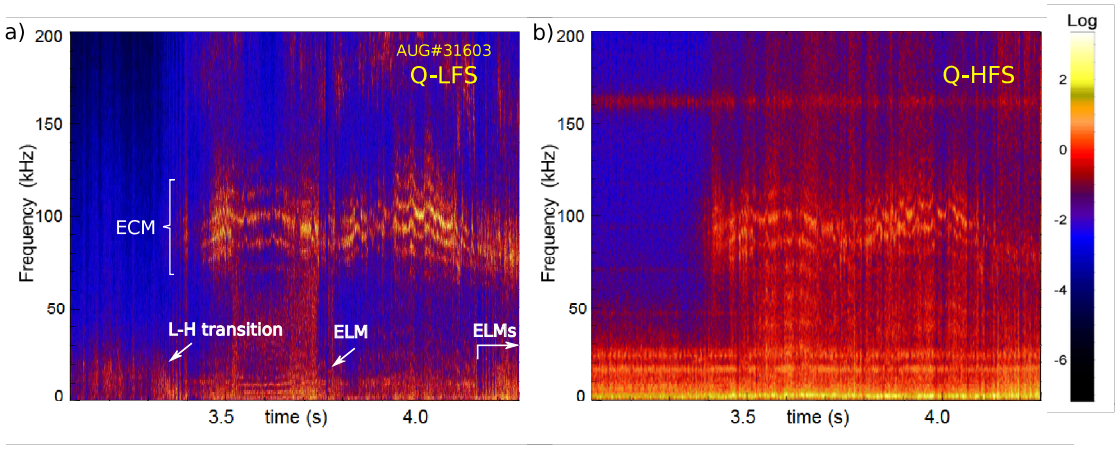

Figure 5. Spectrogram of phase fluctuations in the pedestal region during ELM-free phase of the H-mode reconstructed from the fixed frequency reflectometer signal with $F_{prob} = 39$ GHz (a) from the LFS and (b) from the HFS

3.2. Edge coherent modes throughout the discharge

In an ELM-free phase of an H-mode the observation of ECMs is more convenient as the plasma is perturbed neither by I-phase bursts nor by ELMs. Usually the ECMs are simultaneously visible on the spectrogram of the fixed frequency reflectometer phase and magnetic pick-up coil signals where the different frequency branches are well distinguishable.

In the fixed frequency reflectometer spectrograms the modes are visible in the edge region $0.95 < \rho_{pol} < 1$ at several O-mode frequencies of 22, 36, 39 and 50 GHz both from the low and high field sides of the torus (see Fig. 5a for $F_{prob} = 39$ GHz from the LFS and Fig. 5b from the HFS). 22 GHz corresponds to density $0.6{\cdot}10^{19}$ m^{-3} located in the SOL, for this channel the amplitude of oscillations is very weak and the frequency peak looses its coherence. The presence of a weak peak around the same frequency in the divertor current spectrum suggests that it could be an effect on the transport by the modes located in the pedestal region. The displacement of the cutoff layer causes the disappearance of modes from the spectra. The amplitudes are slightly stronger at the low field side, but this may also be linked to the difference in the channel sensitivities. Therefore the absolute calibration of the FM-CW reflectometer channels is needed to draw a conclusion. The modes appear distinctly 80 ms after the transition to the H-mode (at $t = 3.32$ s), saturate until the first solitary ELM arrives at $t = 3.75$ s and disappear afterwards. After the ELM the mode amplitude starts to grow again until the next regular type-I ELMs ($t = 4.2$ s).

From the UFSR data the modes were observed in a narrow radial region $0.95 < \rho_{pol} < 0.99$ with the strongest branch around 100 kHz (Fig. 6b). The spectrogram in Fig. 6 shows an average of 3 spectra within the time window 3.577–3.561 s calculated for 500 sweeps each. The average spectrum of the complex signal is asymmetric between positive and negative frequencies, which indicates that the shape of the density perturbation is rather sawtooth-like. A poloidal tilt angle of the mode structure might

provide an explanation of this spectra signature [27].

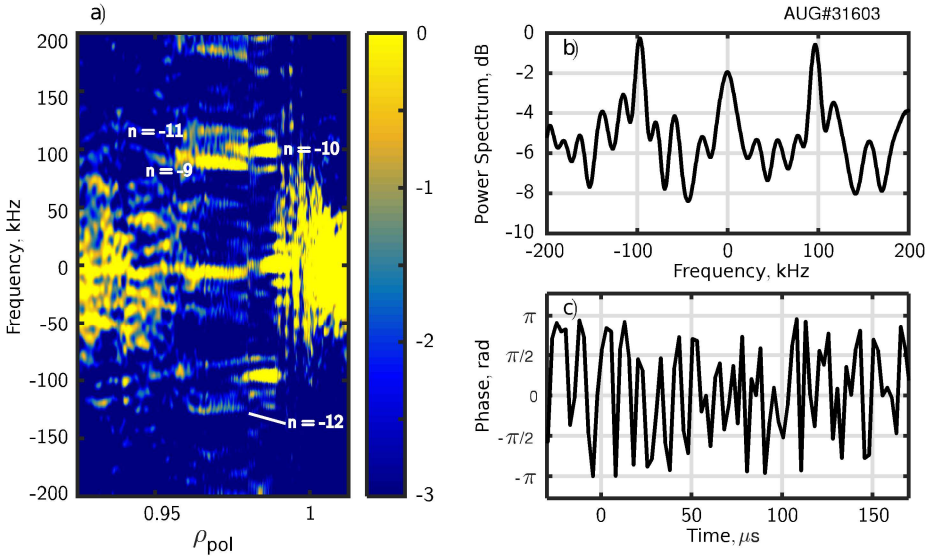

Figure 6. (a) Density fluctuation frequency power spectra during the ELM-free phase of the H-mode t =3.557–3.561 s, (b) a frequency power spectrum at F_{prob} = 69.8 GHz, ρ_{pol} = 0.98 and (c) the reflectometer signal phase showing a 100 kHz oscillation. The mode numbers have been estimated from the PCR data

Looking at the spectrum (Fig. 6b) at one probing frequency, the main branch at 100 kHz with the width of about 5 kHz is visible with the side branches of 85 and 115 kHz . The reflectometer phase shows sequences of oscillations (Fig. 6c) with a period about 7–11 μs, with 5–20 periods each. In the frequency spectrum this bursty behaviour manifests as a broadening of the ECM peaks for longer FFT time windows. This behaviour is observed both in I-phase and H-mode discharges.

In between ELM crashes the ECMs recover and the UFSR sweep rate allows to follow their time evolution. The time between two consecutive ELMs of 1–10 milliseconds allows to calculate a few FFT in different phases of the ELM cycle. Figures 7d–f depict the ECM evolution during ELMs for three time windows. Figure 7g shows the pedestal top density evolution during two consecutive ELMs. The FFT is calculated with windows of 1000 reflectometer sweeps of 2.5 μs each (Figs. 7d–f). The ECMs have frequencies of about 80 and 100 kHz and their amplitude varies from saturation to disappearance during the ELM relaxation of the pedestal, or after a sequence of frequent ELMs. The radial position of the modes is located in the region $0.93 < \rho_{pol} < 0.99$, corresponding to the top of the pedestal and the upper part of the gradient region as it is seen on Fig. 7a,b where the average density profiles are shown for each of 2.5 ms time window. A similar kind of modes is investigated in detail in [6] as MHD activity with several branches with $n < 12$ and fixed f/n values. These modes were located in the pedestal region close to the separatrix from a comparison to the edge plasma rotation. However, the exact position of the modes was not found due to large uncertainties in the estimate of the plasma rotation velocity and equilibrium close to the separatrix [6]. Using the ELM synchronization in the same work, it was shown that dominant toroidal mode numbers sometimes change from high to low n prior to

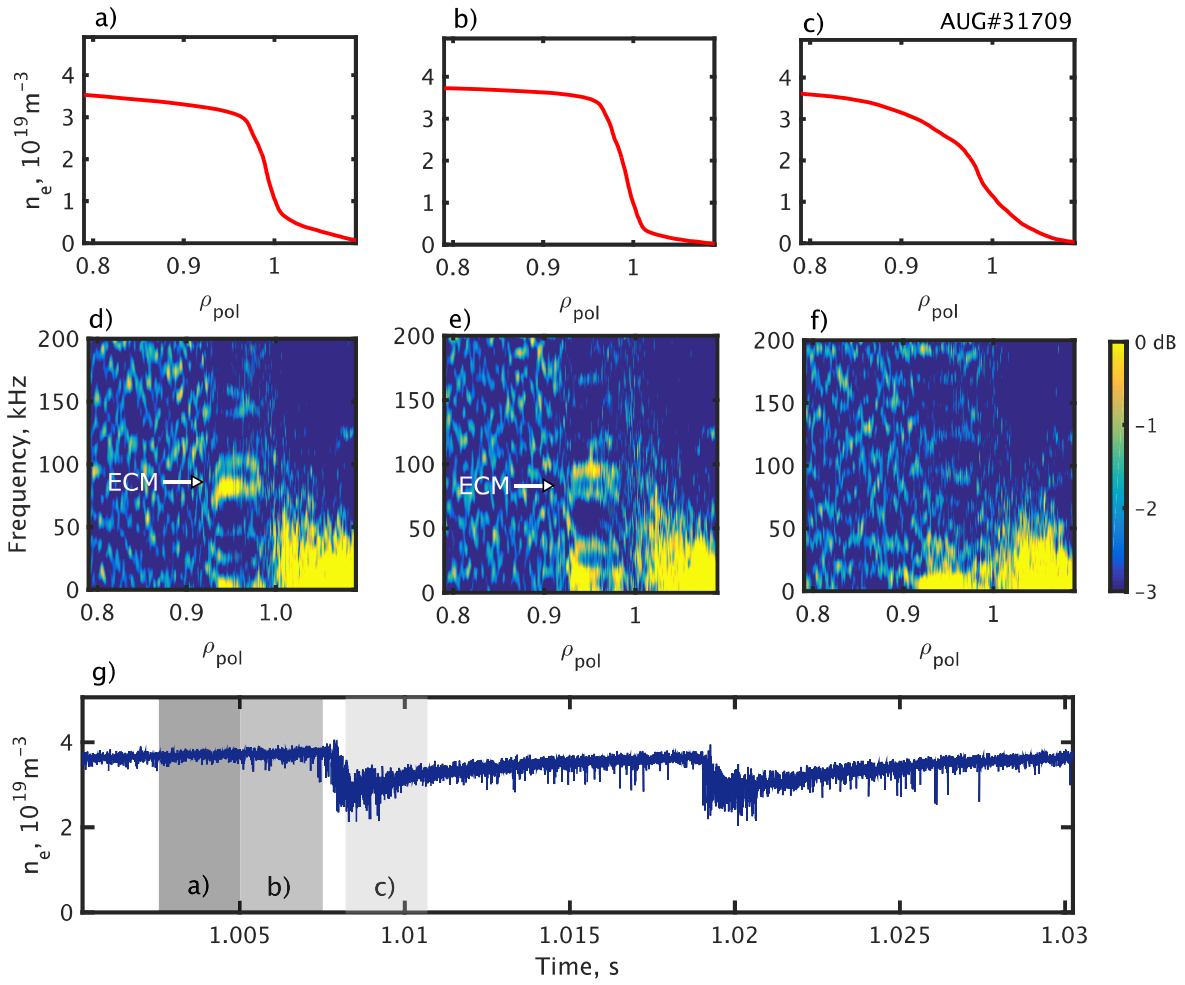

Figure 7. Density profiles (a–c) and density fluctuation frequency power spectra (d–f) during three phases of an ELM cycle indicated with grey areas (g) on the pedestal top denisty evolution ($\rho_{pol} = 0.95$)

the ELM crash [28]. The frequency of the ECMs does not change by more than 5 kHz in between ELMs, a drop of the frequency can be noticed prior to some ELMs.

3.3. Hypotheses on ECM nature

The mode's frequency also lies in the range of the typically observed toroidal Alfvén eigenmodes (TAE) in AUG [23]. The Alfvén frequency is given by

$$f_A = \frac{v_A}{R}\frac{n}{2m+1} \propto q^{-1} {n_i}^{-0.5}, \tag{2}$$

where the Alfvén speed is given by $v_A = B/\sqrt{\mu_0 n_i m_i}$, q is the safety factor, m_i is the ion mass, n_i is the ion density, R is the major radius equal to 1.65 m, μ_0 is vacuum permeability. It is important to note that ECM have been observed in plasmas with both ECR and NBI heating, with only NBI and only ECRH. Hence, the presence of ECMs does not rely on energetic ions which usually excite TAEs. Note also, that there

have been observations of TAE in Ohmically heated AUG plasmas [29]. A possible explanation of the excitation of Alfven modes without energetic ions is the coupling to short wavelength drift Alfven turbulence.

In a nonuniform system, the shear Alfven wave frequency constitutes a continuous spectrum with several branches corresponding to the different values of the toroidal and poloidal mode number. The continuous spectrum has gaps, where Alfven eigenmodes can exist practically unaffected by continuum damping [30]. The frequency of the TAE gap centre can be approximated as $f_{TAE} = f_A/2$ when neglecting the plasma compressibility. For the discharge #31287, the value of the resulting centre of the TAE gap is $f_{TAE} = 95$ kHz in the pedestal region. Here, the compressible effects have been included with the formula described in [31]. A qualitative picture of the continuous spectrum in the discharge #31287 at $t = 2.14$ s, i.e. during the I-phase, has been derived using the approximated formula of [32]. The ECMs are observed to fall inside the TAE gap in the edge region $0.9 < \rho_{pol} < 1$. If we restrict to this consideration only, this means that we cannot exclude that the observed ECMs are TAEs.

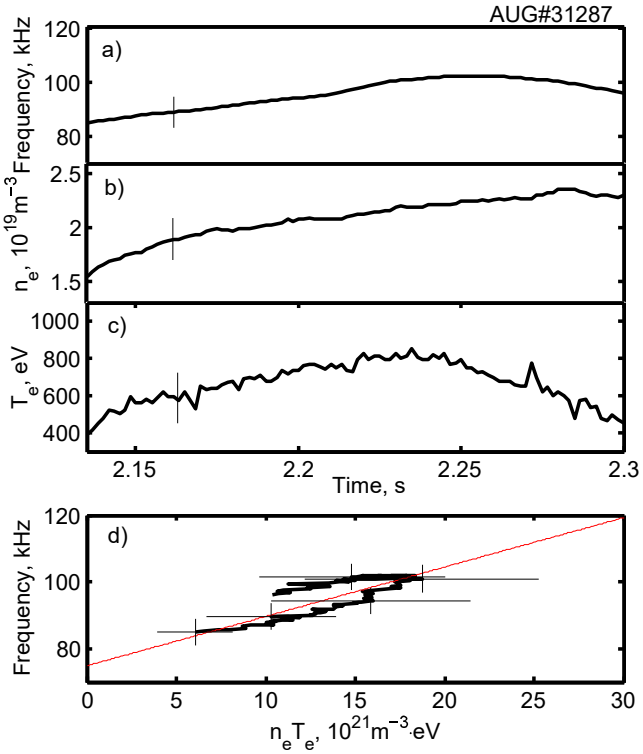

Figure 8. (a) Frequency evolution for the $n = -8$ ECM compared to (b) the edge electron density, (c) temperature and (d) electron pressure dependence of frequency at $\rho_{pol} = 0.97$ in the discharge #31287

From the same discharge the temporal evolution of the mode frequency (Fig. 8a) has been compared to the density and temperature dynamics. Figure 8 depicts the evolution of the electron density (b) and temperature (c) at the top of the pedestal from Thomson scattering during 170 ms of the discharge after the L-H transition. The frequency of the ECM with toroidal mode number $n = -7$ measured with pick-up coils

follows the temperature and density dynamics, although the temperature is changing faster than the ECM frequency, while the density starts to decrease later. The frequency of the mode does not follow the $n_i{}^{-0.5}$ dependence of the Alfvén frequency and this seem to play against the possibility of the ECMs being TAEs, although the TAE frequency can also be modified by the drive, for a fixed Alfvén velocity. We recall nevertheless that these are ECRH discharges, and therefore no energetic particles are present, which represent the typical TAE drive. The data is consistent with a density and temperature dependence as $f \propto n_e T_e$, where the electron pressure is taken at the top of the pedestal (Fig. 8d), which can be a rough estimate for the pressure gradient, assuming the pedestal width is not changing much. Note that the MTM frequency scales with the sum of $\mathbf{E} \times \mathbf{B}$ and electron diamagnetic velocities also proportional to the electron pressure gradient.

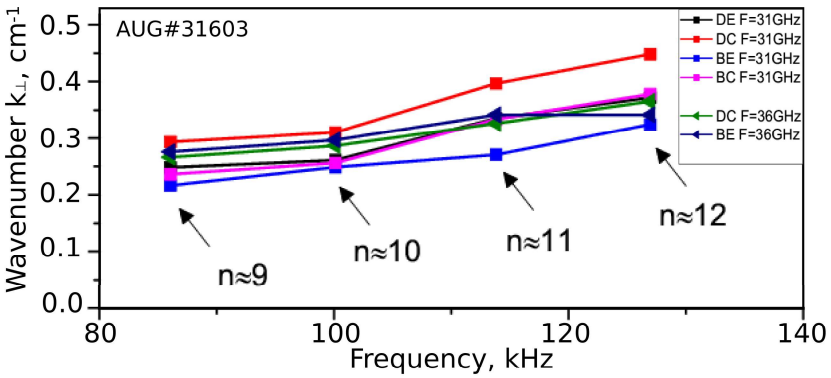

Figure 9. Wavenumbers determined with the PCR for different pairs of antennas B, C, D and E [21] and frequencies of the probing wave of 31 and 36 GHz, corresponding to $\rho_{pol} = 0.98$ and 0.97 respectively

Using different pairs of the poloidal correlation reflectometer (PCR) antennas, the perpendicular wavenumber and the mode number can be estimated from the correlation length for modes with frequencies of 83, 100, 113 and 127 kHz (Fig. 9). The calculation has been done for probing frequencies of 31 and 36 GHz, corresponding to the radial positions $\rho_{pol} = 0.98$ and 0.97. Toroidal mode numbers vary from $n = -9$ to -12, confirming the propagation in the electron diamagnetic direction. The perpendicular wavenumbers are of the order of 0.2–0.4 cm^{-1}. Using the electron temperature measurements, the normalized poloidal wavenumber of the mode is about $k_\theta \rho_s \approx 0.05$ which corresponds to the range of RBM, KBM or MTM. The perpendicular velocity can be estimated as $v_\perp = 23 \pm 5$ km/s. For a typical H-mode in AUG, the profile of the radial electric field has its minimum around $\rho_{pol} = 0.99$ [33]. The corresponding $\mathbf{E} \times \mathbf{B}$ velocity can be estimated through the diamagnetic term of $\mathbf{E_r}$ for the given discharge and is about 15 km/s. E_r changes its sign from negative in the pedestal region to positive in the plasma core, therefore the $\mathbf{E} \times \mathbf{B}$ velocity of the plasma changes its direction from the electron diamagnetic to the ion diamagnetic velocity direction.

The ECMs propagate in the electron diamagnetic direction in the laboratory frame. If they are located at the top of the pedestal where the $\mathbf{E} \times \mathbf{B}$ velocity is low, the modes

also propagate in the electron diamagnetic direction in the plasma frame, which would indicate microtearing modes (MTM) [34]. If the ECMs are located substantially in the region of large $\mathbf{E} \times \mathbf{B}$ velocities, their phase velocity would be small, which is a characteristic for resistive ballooning modes (RBM) [34]. The first hypothesis would be consistent with the gyrokinetic simulations which have shown that MTM can be a dominant instability responsible of the transport at the pedestal top [35]. The formation of the pedestal has been described as an interplay between the MTMs regulating the temperature gradient and transport inside the pedestal and the KBMs limiting the density gradient in the pedestal foot [36]. It is possible that first the MTMs are destabilised at the top of the pedestal during the I-phase and the ELM-free H-mode and that they are not visible in the pick-up coil signal because the level of magnetic fluctuations is low [34]. Then the KBMs are driven at the pedestal foot and thus are detectable with Mirnov coils.

4. Conclusions

The observation of ECMs during L-H transitions led to a more detailed documentation of the edge modes in ASDEX Upgrade in the range of 50–200 kHz. The ECMs are visible in the reflectometer and magnetic pick-up coil spectra and have several well reproducible properties. The UFSR data allow to locate the modes in the plasma edge $0.93 < \rho_{pol} < 0.99$ and, from the comparison between the probing frequencies and density profiles, from the pedestal top to the gradient region. The radial range in which the modes are detected might be broader than the actual size of the mode due to the radial motion of the entire plasma profile. Through a detailed analysis it is shown that the ECM frequency increases with plasma edge electron pressure. ECMs have low toroidal numbers between $n = -5$ and -12 and propagate in the electron diamagnetic direction. From the analysis of the wavenumber spectra it follows that the ECMs have a small radial wavenumber $k_r < 2$ cm^{-1}. The perpendicular wavenumber is about $k_\perp = 0.2$–0.4 cm^{-1}. The fixed frequency reflectometer channels detect the ECM both on the LFS and the HFS, although the absence of absolute sensitivity calibration of different channels does not allow to exclude a strong ballooning character. The modes often have an intermittent character with sequences of 5–20 oscillations observed first in the reflectometry phase signal and only when the ECMs are saturated, in the magnetic pick-up coil signal.

The observation of ECMs in discharges additionally heated by microwaves only (ECRH) indicates that their existence does not depend on energetic particles. This fact, together with the linear frequency dependence on the electron density, excludes the hypothesis of a toroidal Alfvén eigenmode. The propagation approximately with the electron diamagnetic velocity and the localisation close to the pedestal top would be consistent with microtearing modes as source of the observed coherent fluctuations. However, as the modes are observed mainly in the gradient region, where the $\mathbf{E} \times \mathbf{B}$ velocity is also of the order of the electron diamagnetic velocity, a small phase velocity

would also be consistent with the observations. This would then indicate to resistive ballooning modes as source of the coherent modes. The impact of ECMs on plasma confinement is an issue that needs to be investigated in the future.

Acknowledgments

The authors wish to especially thank L.Gil and P. Lauber for fruitful discussions and valuable comments. This work has been carried out within the framework of the Erasmus Mundus International Doctoral College in Fusion Science and Engineering. It has received funding from the Euratom research and training programme 2014-2018 and 2019-2020 under grant agreement No 633053. The views and opinions expressed herein do not necessarily reflect those of the European Commission. This work was also performed within the framework of the Helmholtz Virtual Institute on Plasma Dynamical Processes and Turbulence Studies using Advanced Microwave Diagnostics.

[1] Smeulders P, Conway G, Alper B, Balet B, Bartlett D, Borba D, Deliyanakis N, Hender T and Kwon O 1999 *Plasma physics and controlled fusion* **41** 1303

[2] Burrell K H, Austin M, Brennan D, DeBoo J, Doyle E, Gohil P, Greenfield C *et al.* 2002 *Plas. Phys. and Cont. Fusion* **44** A253

[3] Suttrop W, Maraschek M, Conway G, Fahrbach H, Haas G, Horton L, Kurki-Suonio T, Lasnier C, Leonard A, Maggi C *et al.* 2003 *Plas. Phys. and Cont. Fusion* **45** 1399

[4] Yan Z, McKee G, Groebner R, Snyder P, Osborne T and Burrell K 2011 *Phys. Rev. Lett.* **107** 055004

[5] Laggner F M, Wolfrum E, Cavedon M, Mink F, Viezzer E, Dunne M G, Manz P, Doerk H, Birkenmeier G, Fischer R, Fietz S, Maraschek M, Willensdorfer M, Aumayr F, the EUROfusion MST1 Team and the ASDEX Upgrade Team 2016 *Plas. Phys. and Cont. Fusion* **58** 065005

[6] Mink F, Wolfrum E, Maraschek M, Zohm H, Horváth L, Laggner F M, Manz P, Viezzer E, Stroth U *et al.* 2016 *Plas. Phys. and Cont. Fusion* **58** 125013

[7] Mazurenko A, Porkolab M, Mossessian D, Snipes J A, Xu X Q and Nevins W M 2002 *Phys. Rev. Lett.* **89**(22) 225004

[8] Zhong W, Zou X, Shi Z, Duan X, Xu Y, Xu M, Chen W, Jiang M, Yang Z, Zhang B *et al.* 2016 *Plasma Physics and Controlled Fusion* **58** 065001

[9] Wang H, Xu G, Wan B, Ding S, Guo H, Shao L, Liu S, Xu X, Wang E, Yan N *et al.* 2014 *Phys. Rev. Lett.* **112** 185004

[10] Diallo A, Groebner R, Rhodes T, Battaglia D, Smith D, Osborne T, Canik J M, Guttenfelder W and Snyder P 2015 *Phys. Plasmas* **22** 056111

[11] Diallo A, Hughes J, Greenwald M, LaBombard B, Davis E, Baek S, Theiler C, Snyder P, Canik J, Walk J *et al.* 2014 *Phys. Rev. Lett.* **112** 115001

[12] Snipes J A, LaBombard B, Greenwald M, Hutchinson I, Irby J, Lin Y, Mazurenko A and Porkolab M 2001 *Plas. Phys. and Cont. Fusion* **43** L23

[13] Chang Z, Fredrickson E, Zweben S, Park H, Nazikian R, Mazzucato E, Batha S *et al.* 1995 *Nucl. Fusion* **35** 1469

[14] Conway G D, Angioni C, Ryter F, Sauter P and Vicente J 2011 *Phys. Rev. Lett.* **106** 065001

[15] Birkenmeier G, Cavedon M, Conway G, Manz P, Stroth U, Fischer R, Fuchert G, Happel T, Laggner F, Maraschek M *et al.* 2016 *Nucl. Fusion* **56** 086009

[16] Igochine V *et al.* 2015 *Active control of magneto-hydrodynamic instabilities in hot plasmas* (Springer)

[17] Cupido L, Graca S, Conway G, Manso M, Serra F and Team A U 2006 *Rev. Sci. Instrum.* **77** 10E915

[18] Clairet F, Bottereau C, Medvedeva A, Molina D, Conway G, Silva A, Stroth U, Team A U, Team T S and Team E M 2017 *Rev. Sci. Instrum.* **88** 113506
[19] Bottollier-Curtet H and Ichtchenko G 1987 *Rev. Sci. Instrum.* **58** 539–546
[20] Heuraux S, Hacquin S, da Silva F, Clairet F, Sabot R and Leclert G 2003 *Rev. Sci. Instrum.* **74** 1501–1505
[21] Prisiazhniuk D, Krämer-Flecken A, Conway G, Happel T, Lebschy A, Manz P, Nikolaeva V, Stroth U *et al.* 2017 *Plas. Phys. and Cont. Fusion* **59** 025013
[22] Medvedeva A, Bottereau C, Clairet F, Hennequin P, Stroth U, Birkenmeier G, Cavedon M, Conway G, Happel T, Heuraux S *et al.* 2017 *Plas. Phys. and Cont. Fusion* **59** 125014
[23] García-Muñoz M, Hicks N, van Voornveld R, Classen I, Bilato R, Bobkov V, Bruedgam M, Fahrbach H U, Igochine V *et al.* 2010 *Phys. Rev. Lett.* **104** 185002
[24] Da Graca S, Conway G, Lauber P, Maraschek M, Borba D, Günter S, Cupido L, Sassenberg K *et al.* 2007 *Plas. Phys. and Cont. Fusion* **49** 1849
[25] Medvedeva A 2017 *Experimental study of turbulence at the plasma edge of ASDEX Upgrade tokamak with an ultra-fast swept reflectometer* Ph.D. thesis Université de Lorraine ; Technische Universität München URL `https://d-nb.info/1148650113/34`
[26] Mink F, Wolfrum E, Maraschek M, Zohm H, Horváth L, Viezzer E, Laggner F, Dunne M, Manz P, Stroth U *et al.* 2016 Characterization of inter-elm magnetic oscillations on asdex upgrade *43rd EPS Conference on Plasma Physics* (European Physical Society)
[27] Clairet F, Medvedeva A, Bottereau C, Dif-Pradalier G, Garbet X, Stroth U, Meneses L, Team A U, Contributors J, Team E M *et al.* 2018 Shear effect on edge turbulence during the lh transition in jet and asdex upgrade plasmas *45th EPS Conference on Plasma Physics*
[28] Mink A, Hoelzl M, Wolfrum E, Orain F, Dunne M, Lessig A, Pamela S, Manz P, Maraschek M, Huijsmans G *et al.* 2017 *Nucl. Fusion* **58** 026011
[29] Maraschek M, Günter S, Kass T, Scott B, Zohm H and Team A U 1997 *Phys. Rev. Lett.* **79** 4186
[30] Chen L and Hasegawa A 1974 *The Physics of Fluids* **17** 1399–1403
[31] Novikau I, Biancalani A, Bottino A, Conway G, Gürcan Ö, Manz P, Morel P, Poli E, Di Siena A and Team A U 2017 *Phys. Plasmas* **24** 122117
[32] Biancalani A, Bottino A, Briguglio S, Könies A, Lauber P, Mishchenko A, Poli E, Scott B and Zonca F 2016 *Phys. Plasmas* **23** 012108
[33] Viezzer E, Pütterich T, Conway G, Dux R, Happel T, Fuchs J, McDermott R, Ryter F, Sieglin B, Suttrop W, Willensdorfer M, Wolfrum E and the ASDEX Upgrade Team 2013 *Nucl. Fusion* **53** 053005
[34] Manz P, Boom J, Wolfrum E, Birkenmeier G, Classen I, Luhmann Jr N, Stroth U *et al.* 2014 *Plas. Phys. and Cont. Fusion* **56** 035010
[35] Hatch D, Kotschenreuther M, Mahajan S, Valanju P and Liu X 2017 *Nucl. Fusion* **57** 036020
[36] Dickinson D, Roach C, Saarelma S, Scannell R, Kirk A and Wilson H 2012 *Phys. Rev. Lett.* **108** 135002